Measurement of the Michel Parameter ρ in Muon Decay

J.R. Musser,[6] R. Bayes,[7, *] Yu.I. Davydov,[7, †] P. Depommier,[4] J. Doornbos,[7] W. Faszer,[7] C.A. Gagliardi,[6]
A. Gaponenko,[1] D.R. Gill,[7] P. Green,[1] P. Gumplinger,[7] M.D. Hasinoff,[2] R.S. Henderson,[7] J. Hu,[7]
B. Jamieson,[2] P. Kitching,[1] D.D. Koetke,[8] A.A. Krushinsky,[3] Yu.Yu. Lachin,[3] J.A. Macdonald,[7, ‡]
R.P. MacDonald,[1] G.M. Marshall,[7] E.L. Mathie,[5] L.V. Miasoedov,[3] R.E. Mischke,[7] P.M. Nord,[8]
K. Olchanski,[7] A. Olin,[7, *] R. Openshaw,[7] T.A. Porcelli,[7, §] J.-M. Poutissou,[7] R. Poutissou,[7]
M.A. Quraan,[1] N.L. Rodning,[1, ‡] V. Selivanov,[3] G. Sheffer,[7] B. Shin,[7, ¶] F. Sobratee,[1]
T.D.S. Stanislaus,[8] R. Tacik,[5] V.D. Torokhov,[3] R.E. Tribble,[6] M.A. Vasiliev,[6] and D.H. Wright[7, **]

(TWIST Collaboration)

[1] *University of Alberta, Edmonton, AB, T6G 2J1, Canada*
[2] *University of British Columbia, Vancouver, BC, V6T 1Z1, Canada*
[3] *Kurchatov Institute, Moscow, 123182, Russia*
[4] *University of Montreal, Montreal, QC, H3C 3J7, Canada*
[5] *University of Regina, Regina, SK, S4S 0A2, Canada*
[6] *Texas A&M University, College Station, TX 77843, U.S.A.*
[7] *TRIUMF, Vancouver, BC, V6T 2A3, Canada*
[8] *Valparaiso University, Valparaiso, IN 46383, U.S.A.*
(Dated: February 2, 2005)

The TWIST Collaboration has measured the Michel parameter ρ in normal muon decay, $\mu^+ \rightarrow e^+ \nu_e \bar{\nu}_\mu$. In the Standard Model, $\rho = 3/4$. Deviations from this value imply mixing of left- and right-handed muon and electron couplings. We find $\rho = 0.75080 \pm 0.00032(\text{stat.}) \pm 0.00097(\text{syst.}) \pm 0.00023$, where the last uncertainty represents the dependence of ρ on the Michel parameter η. This result sets new limits on the $W_L - W_R$ mixing angle in left-right symmetric models.

PACS numbers: 13.35.Bv, 14.60.Ef, 12.60.Cn

Normal muon decay, $\mu^+ \rightarrow e^+ \nu_e \bar{\nu}_\mu$, is an excellent laboratory to test the space-time structure of the weak interaction. The energy and angular distributions of the positrons emitted in the decay of polarized muons can be described in terms of four parameters – ρ, η, ξ, and δ – commonly referred to as the Michel parameters. Neglecting the electron and neutrino masses and radiative corrections, the differential decay rate for positive muon decay is given in terms of ρ, ξ, and δ by [1]:

$$\frac{d^2\Gamma}{x^2 dx d(\cos\theta)} \propto (3 - 3x) + \frac{2}{3}\rho(4x - 3)$$
$$+ P_\mu \xi \cos\theta \left[(1 - x) + \frac{2}{3}\delta(4x - 3) \right], \quad (1)$$

where P_μ is the polarization of the muon, $x = E_e/E_{e,max}$, and θ is the angle between the muon polarization axis and the positron decay direction. The fourth decay parameter, η, contributes to the angle-independent part of the distribution if one includes the finite electron mass. In this Letter, the TWIST Collaboration reports a new measurement of the Michel parameter ρ. A concurrent measurement of the parameter δ is described in Ref. [2].

The current accepted value of ρ, 0.7518 ± 0.0026 [3, 4], is consistent with the Standard Model expectation, $\rho = 3/4$. Any deviation from $3/4$ would imply the muon-decay Lagrangian includes scalar, vector, or tensor couplings between left-handed muons and right-handed electrons or vice versa [5]. For example, in left-right symmet-

ric models, the $W_L - W_R$ mixing angle ζ is given by [6]

$$\zeta = \sqrt{\frac{2}{3}\left(\frac{3}{4} - \rho\right)}. \quad (2)$$

Unlike many other limits on right-handed currents, this is independent of the form of the right-handed CKM matrix. Recently, ρ has also been related to loop corrections to the neutrino mass matrix [7]. For a review of muon decay within the Standard Model, see Ref. [8].

TWIST utilizes the M13 beam line at TRIUMF to transport beams of 29.6 MeV/c surface muons from pion decay-at-rest ($P_\mu \sim -1$) or 32.8 MeV/c cloud muons from pion decay-in-flight ($P_\mu \sim +0.25$) into the TWIST spectrometer. The TWIST spectrometer consists of an array of very thin, high precision planar wire chambers located within a 2-T magnetic field oriented along the beam direction. The spectrometer includes 44 drift chamber (DC) planes operated with DME gas and 12 fast multi-wire proportional chamber (PC) planes. The wire planes are symmetrically located upstream and downstream of a 125-μm thick Mylar stopping target, with 10^{+10}_{-5} μm of graphite painted on each surface. A detailed description of the TWIST spectrometer is given in Ref. [9].

After muons enter the magnetic field, they pass through a thin plastic trigger scintillator. They then pass through detector planes; $\sim 80\%$ stop in the target. Decay positrons follow helical trajectories through the DCs and PCs, permitting their momenta and decay angles to be

measured precisely. For each event, all DC and PC hits within an interval from 6 μs before until 10 μs after the trigger time are recorded.

During off-line analysis, the PC and DC hits are examined to identify events in which the muon stopped in the target, then decayed at least 1.05 μs, and no more than 9 μs, later. The delay insures that the PC and DC hits associated with the muon and decay positron do not overlap. Events are rejected if a second muon enters the spectrometer, or if a beam positron passes through within 1.05 μs of either the muon arrival or decay time. The muon beam rate was 2500/s; the positron rate was 22,000/s. Additional cuts include the muon flight time through the M13 beam line and a requirement that the muon stopping location be within 2.5 cm of the detector axis. All events that pass these cuts are analyzed to reconstruct the decay positron kinematics.

After track fitting, 2.3% of the events contain additional tracks in coincidence with the decay. Extra tracks can arise from beam particles that are not resolved in time, events that scatter within the detector leading to two reconstructed track segments, and events that include delta rays or decay positrons that backscatter from material outside the detector volume. Two algorithms have been developed to select among the choices in multi-track events. They also impose different constraints on events that scatter within the detector when only one track segment is reconstructed. All events have been analyzed using both algorithms.

To extract the Michel parameters, the measured positron momentum-angle spectrum is compared to that predicted by a detailed Monte Carlo (MC) simulation. The MC uses GEANT [10] to simulate particle interactions and a model based on GARFIELD [11] to simulate wire chamber responses. The MC decay generator includes the effects of electron mass, plus first-order and many higher-order radiative corrections [12]. It also includes beam positrons and additional muons in the simulated events according to their observed rates in the data. The output from the MC is digitized and processed by the same analysis codes that are used for real events.

The data reported here include a total of 6×10^9 muon decay events that were recorded during Fall, 2002. Sixteen independent data sets were taken to explore the sensitivity of the spectrometer and analysis to a broad range of systematic effects. A typical data set included 3×10^8 events, sufficient to determine ρ with a statistical precision of ~ 0.0007. In addition, special runs were taken to provide data to validate aspects of the simulation that are difficult to test with the muon decay spectrum. Five data sets were taken under conditions that permit a reliable determination of ρ. Four sets were taken with a surface muon beam. Sets A and B were obtained six weeks apart at a magnetic field of 2.00 T; the other sets were taken at 1.96 T and 2.04 T. The fifth data set was taken at 2.00 T with a cloud muon beam to verify the independence
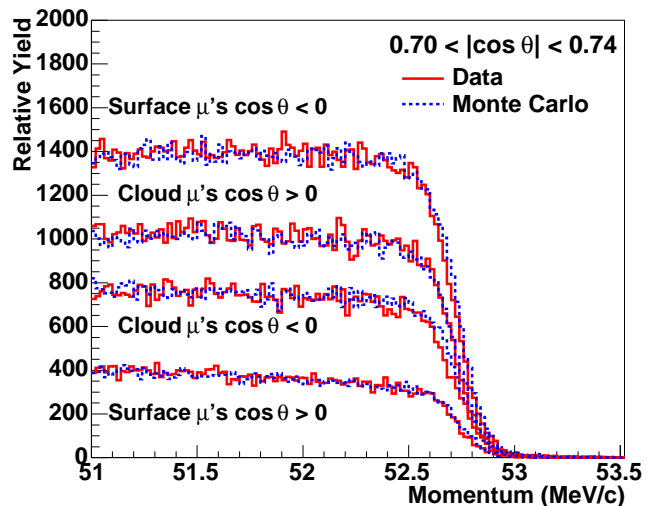

FIG. 1: (color online) Measured positron momenta (solid lines) near the end point are compared to Monte Carlo simulations (dotted lines). The curves show surface muon set B and cloud muon spectra for $0.70 < |\cos\theta| < 0.74$.

of ρ on beam polarization. Depolarizing interactions in the target reduced the average muon polarization at the time of decay to $\sim 90\%$ of the incident polarization.

The only discrete feature in the muon decay spectrum is the end point. Figure 1 shows comparisons of the measured spectra near the end point to MC simulations. The typical momentum resolution is ~ 100 keV/c. The observed end point falls below the kinematic limit of 52.828 MeV/c due to positron energy loss in the target and detector materials. Fits to spectra in the region $p > 52$ MeV/c show that the energy loss follows the form, $\Delta E(\theta) = -\alpha/|\cos\theta|$, with α a constant as expected for the planar geometry of the TWIST detectors [13]. α takes on different values for upstream and downstream decays when the muon stopping distribution is not centered in the target. Typically α is ~ 75 keV. We use $E = E_{meas} + \alpha/|\cos\theta|$ to correct both data and MC events for the average positron energy loss.

Effects that distort the reconstructed positron momenta will lead to systematic errors in the value of ρ if they are not simulated accurately by the MC. To test the simulation of energy loss for positron momenta well below 52.83 MeV/c, events were recorded in which a muon came to rest at the far upstream end of the detector. Positrons from muon decays in the downstream direction first spiral through the upstream half of the detector, then pass through the target and spiral through the downstream half. Figure 2 shows the difference between the reconstructed positron momenta in the two halves, which measures the energy loss in the target and detector materials. The MC agrees very well with the data. Similar comparisons verify the MC simulation of positron multiple scattering [2] and hard interaction rates.
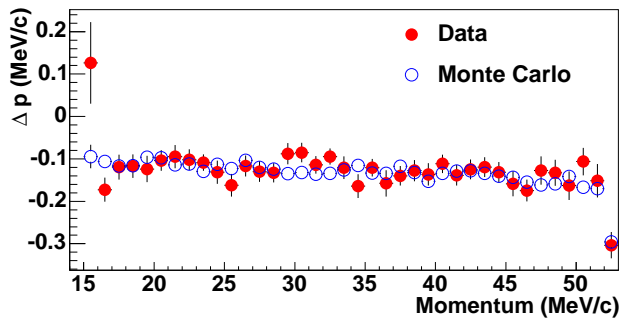
FIG. 2: (color online) Average momentum change of decay positrons through the target and detector materials as a function of momentum for data (closed circles) and Monte Carlo (open circles), measured as described in the text.

If $\rho = \rho_H + \Delta\rho$ and $\eta = \eta_H + \Delta\eta$, then the angle-integrated muon decay spectrum can be written as:

$$N(x) = N_S(x, \rho_H, \eta_H) + \Delta\rho N_{\Delta\rho}(x) + \Delta\eta N_{\Delta\eta}(x). \quad (3)$$

This expansion is exact. It can also be generalized to include the angular dependence [2]. This is the basis for the blind analysis. The measured momentum-angle spectrum is fitted to the sum of a MC 'standard' spectrum N_S produced with unknown Michel parameters ρ_H, η_H, ξ_H, δ_H and additional 'derivative' MC distributions $N_{\Delta\rho}$, $N_{\Delta\xi}$, and $N_{\Delta\xi\delta}$, with $\Delta\rho$, $\Delta\xi$, and $\Delta\xi\delta$ as the fitting parameters. The hidden Michel parameters associated with N_S are revealed only after all data analysis has been completed. The fiducial region adopted for this analysis requires $p < 50$ MeV/c, $|p_z| > 13.7$ MeV/c, $p_T < 38.5$ MeV/c, and $0.50 < |\cos\theta| < 0.84$.

Fits over this momentum range including both ρ and η contain very strong correlations [3]. To optimize the precision for ρ, η was fixed at the hidden value η_H throughout the blind analysis, then a refit was performed to shift η to the accepted value. We find that ρ depends linearly on the assumed value of η, with $d\rho/d\eta = 0.018$.

Figure 3(a) shows the momentum spectrum from set B in the angular range $0.70 < |\cos\theta| < 0.84$. The probability for reconstructing muon decays is very high, as shown in Figs. 3(b) and (d). Thus, higher momentum decays that undergo hard interactions and are reconstructed at lower momenta can lead to an apparent reconstruction probability above unity. Figures 3(c) and (e) show the residuals of the fit of the decay spectrum from set B. Similar fits have been performed to the other data sets, yielding the results shown in Table I. The fit results for δ are not adopted due to a problem with the polarization-dependent radiative corrections in the event generator [2], but are consistent with the separate analysis reported in [2]. Fits to the angle-integrated spectra, which are independent of δ, give nearly identical results for ρ.

The 11 additional data sets have been combined with further MC simulations to estimate the systematic uncertainties shown in Tables I and II. The largest effects
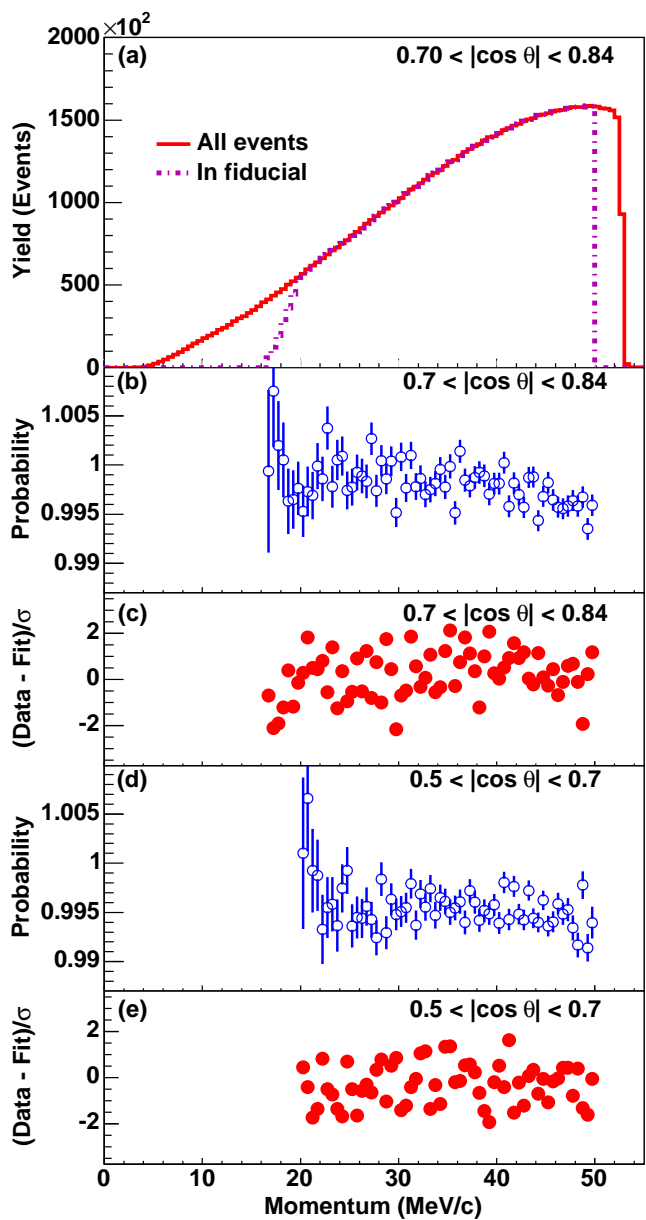

FIG. 3: (color online) Panel (a) shows the muon decay spectrum (solid curve) from surface muon set B vs. momentum, for events within $0.70 < |\cos\theta| < 0.84$, as well as the events within this angular region that pass the fiducial constraints (dot-dashed curve). The spectrum within $0.5 < |\cos\theta| < 0.7$ is similar. Panels (b) and (d) show the probability for reconstructing decays for the two angular ranges, as calculated by the Monte Carlo. Panels (c) and (e) show the residuals for the same angular ranges from the fit of set B to the Monte Carlo 'standard' spectrum plus derivatives.

arise from time-variations of the cathode foil locations [9] and the density of the DME gas, which change the drift velocities and influence the DC efficiencies far from the sense wires. These parameters were monitored throughout the data taking, but only average values were used in the analysis. Special data sets and MC simulations that

TABLE I: Results from the fits to the various data sets using one of the track selection algorithms. Each fit has 1887 degrees of freedom. Only statistical and set-dependent systematic uncertainties are shown.

Data Set	ρ	χ^2
Set A	$0.75134 \pm 0.00083 \pm 0.00053$	1814
Set B	$0.74937 \pm 0.00066 \pm 0.00053$	1965
1.96 T	$0.75027 \pm 0.00065 \pm 0.00055$	1951
2.04 T	$0.75248 \pm 0.00070 \pm 0.00060$	1804
Cloud	$0.75157 \pm 0.00076 \pm 0.00053$	1993

TABLE II: Contributions to the systematic uncertainty in ρ. Average values are given for those denoted (ave), which are considered set dependent when performing the weighted average of the data sets.

Effect	Uncertainty
Chamber response (ave)	± 0.00051
Stopping target thickness	± 0.00049
Positron interactions	± 0.00046
Spectrometer alignment	± 0.00022
Momentum calibration (ave)	± 0.00020
Theoretical radiative corrections [12]	± 0.00020
Track selection algorithm	± 0.00011
Muon beam stability (ave)	± 0.00004
Total in quadrature	± 0.00093
Scaled total	± 0.00097

amplify these effects have been used to estimate their uncertainties for ρ. Other important effects arise from the uncertainty in the thickness of the graphite layers on the Mylar target [9] and from uncertainties in the GEANT treatment of positron interactions that lead to the spectrum distortions seen in Fig. 3. Upper limits on these uncertainties were obtained from the data where the muons stopped far upstream. Several other effects make smaller contributions, as enumerated in Table II.

We treat the chamber response, momentum calibration, and beam stability uncertainties as set dependent when computing the average of the data sets since the underlying causes fluctuated in time. This gives $\rho = 0.75091 \pm 0.00032$(stat.), with $\chi^2 = 7.5$ for 4 degrees of freedom. We scale the uncertainties to account for the χ^2 value, equivalent to an additional contribution of ± 0.00030. The alternative track selection technique gives $\rho = 0.75069$. We average these results as our best estimate of ρ, and include half the difference in the systematic uncertainty. To be conservative, we consider all systematic uncertainties to be common to the data sets.

We find $\rho = 0.75080 \pm 0.00032$(stat.) ± 0.00097(syst.) ± 0.00023, consistent with the Standard Model expectation $\rho = 3/4$. This result assumes that η is given by the accepted value, $\eta = -0.007 \pm 0.013$ [4, 14]; the third uncertainty represents the change in ρ when η changes within its uncertainty. Within left-right symmetric models, this result sets a new upper limit, $|\zeta| < 0.030$ (90% c.l.), on the $W_L - W_R$ mixing angle.

* Affiliated with: Univ. of Victoria, Victoria, BC.
† Affiliated with: Kurchatov Institute, Moscow, Russia.
‡ Deceased.
§ Present address: Univ. of Manitoba, Winnipeg, MB.
¶ Affiliated with: Univ. of Saskatchewan, Saskatoon, SK.
** Present address: Stanford Linear Accelerator Center, Stanford, CA.

[1] L. Michel, Proc. Phys. Soc. A63, 514 (1950); C. Bouchiat and L. Michel, Phys. Rev. 106, 170 (1957); T. Kinoshita and A. Sirlin, Phys. Rev. 108, 844 (1957).
[2] A. Gaponenko et al. (TWIST Collaboration), hep-ex/0410045.
[3] J. Peoples, Ph.D. thesis, Columbia University, Nevis Report No. 147 (1966), unpublished; B.A. Sherwood, Phys. Rev. 156, 1475 (1967); D. Fryberger, Phys. Rev. 166, 1379 (1968); S.E. Derenzo, Phys. Rev. 181, 1854 (1969).
[4] S. Eidelman et al., Phys. Lett. B592, 1 (2004).
[5] W. Fetscher and H.-J. Gerber, Precision Tests of the Standard Electroweak Model, ed. by P. Langacker (World Scientific, Singapore, 1995), 657.
[6] P. Herczeg, Phys. Rev. D 34, 3449 (1986).
[7] G. Prezeau, A. Kurylov, and M.J. Ramesy-Musolf, hep-ph/0409193.
[8] Y. Kuno and Y. Okada, Rev. Mod. Phys. 73, 151 (2001).
[9] R.S. Henderson et al., hep-ex/0409066.
[10] R. Brun et al., GEANT, version 3.2114.
[11] R. Veenhof, GARFIELD, version 7.10.
[12] A.B. Arbuzov, Phys. Lett. B524, 99 (2002); JHEP 0303, 063 (2003); JTEP Lett. 78, 179 (2003); A. Arbuzov, A. Czarnecki, and A. Gaponenko, Phys. Rev. D 65, 113006 (2002); A. Arbuzov and K. Melnikov, Phys. Rev. D 66, 093003 (2002).
[13] A.A. Khrutchinsky, Yu.Yu Lachin, and V.I. Selivanov, Nucl. Instrum. Meth. A396, 135 (1997).
[14] N. Danneberg et al., Phys. Rev. Lett. 94, 021802 (2005). This result will need to be included in a new global analysis before it can supercede the accepted value from [4].